Proceedings of the 17th World Congress
The International Federation of Automatic Control
Seoul, Korea, July 6-11, 2008

Control and Systems Approaches to Atomic Force Microscopy

Pranav Agarwal * **Murti V. Salapaka** **

* *Electrical and Computer Engineering Department, University of Minnesota, Minneapolis (e-mail: agar0108@umn.edu).*
** *Electrical and Computer Engineering Department, University of Minnesota, Minneapolis (e-mail:murtis@umn.edu).*

Abstract: The atomic force microscope (AFM) and its derivative technologies have heralded a new era in science and technology. AFM and related instruments were primarily designed by physicists. In recent years there is a substantial presence of engineers with controls and systems background who are contributing to AFM related technologies. This article provides a tutorial on the control and systems approaches to AFM. This paper also delineates the impact controls and systems perspectives have on AFM related research and indicates future directions.

1. INTRODUCTION

The invention of scanning tunneling microscope (STM) is a significant event toward realizing the vision of atomic scale interrogation of materials. STM enabled three dimensional imaging of materials with atomic scale resolution. This device is based on *tunneling* where electrons on the surface of a material move into or *tunnel* into the surface of the other material when these surfaces are brought sufficiently close to each other. Earlier tunneling experiments were not successful primarily due to adverse effects of extraneous vibrations. In 1981, G. Binnig and H. Rohrer presented the first successful tunneling experiment with the surfaces separated by vacuum (see Binnig et al. (1982)). Pivotal to the success of this experiment was a feedback loop that controlled the vacuum gap between the probe and the sample surfaces that effectively nulled the effects of the extraneous vibrations. G. Binnig and H. Rohrer were awarded the Nobel prize in physics in 1986 for STM, only four years after their remarkable invention.

STM is limited primarily to conductors and semi-conductors. In 1986, G. Binnig, C.F. Quate, and Ch. Gerber invented the atomic force microscope (AFM) that made it possible to image insulators with atomic resolution. AFM and its derivative instruments, termed scanning probe microscopes (SPMs), provide evidence of the feasibility of control, manipulation, and interrogation of matter at the nanoscale, which is emphasized in the 2000 National Nanotechnology Initiative (NNI) Plan as, "these instruments including STMs, AFMs, and near field microscope provide the eyes and fingers required for nanostructure, manipulation and measurement" (see nni).

Feedback formed an important and integral part of the scanning probes right in their original designs. This article emphasizes the potential of controls and systems tools in providing new insights and modeling techniques for nanoscale phenomena.

⋆ This work was supported in part by the National Science Foundation by the ECS and CMS divisions

The paper is organized as follows. In Section 2, the basic operating principles of the AFM, together with the basic modes of operation and primary components are presented. In Section 3, the systems and controls tools are presented. In Section 4 the main conclusions and future directions are presented.

2. BASIC OPERATING PRINCIPLES

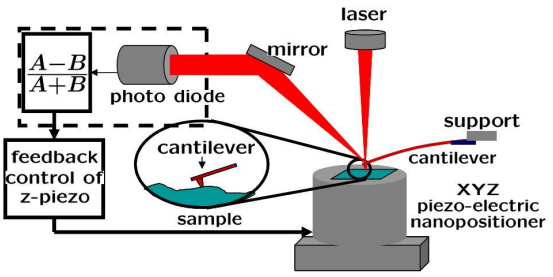

Fig. 1. Atomic force microscope (AFM). The AFM yields atomic resolution imaging capability that can be employed for conductors and insulators unlike the STM. The main probe, a microcantilever, is a force sensor. The deflection of the cantilever is registered by a laser incident on the cantilever, which reflects onto a split photodiode. In most imaging modes, the control signal, which regulates a setpoint by moving the sample vertically relative to the cantilever probe, forms the image of the sample. In most setups, a piezo scanner positions the sample relative to the tip in the lateral and the vertical direction.

The main components of an atomic force microscope are shown in Fig. 1. The main components are (1) A microcantilever probe that has a sharp tip at one end. The supported end can be forced using piezoelectric material (termed the dither piezo). Typical length, width, and thickness of microcantilevers used in AFM are 100 μm, 10 μm, and 2 μm respectively. The stiffness of these microcantilevers vary from 0.06 to 100 N/m (see Sarid (1991)). (2) The detection system that consists of a laser that is

incident on the tip end of the cantilever. The incident laser is reflected into a split photodiode that provides a voltage signal proportional to the difference in the laser power incident on its different halves. (3) The control system takes the measured signal as input and provides the control signal to the nanopositioning device and possibly the cantilever support. (4) The nanopositioning device provides the capability of positioning the sample with respect to the cantilever probe in the lateral x and y directions and the vertical z direction.

2.1 Models of cantilever and the measurement process

The cantilever is often modelled as a spring-mass-damper system with the dynamics described by

$$\ddot{p} + \frac{\omega_0}{Q}\dot{p} + \omega_0^2 p = f(t), \tag{1}$$

and the measured signal y is

$$y = p + \upsilon \tag{2}$$

where p denotes the deflection of the tip, ω_0 is the first modal frequency, Q is the associated quality factor, $f(t)$ is the net force on the cantilever and υ is the measurement noise. The above model can be derived by the first mode approximation of a flexure beam. Typical cantilevers used in AFM have first resonant modal frequencies in the range 10-400 kHz. The quality factors can range from 2 in liquid environment to 10,000 or higher under vacuum.

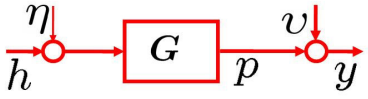

(a)

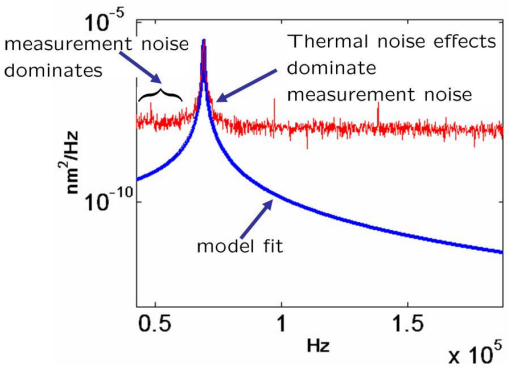

(b)

Fig. 2. (a) Shows a block diagram representation of the cantilever system G being forced by white noise (η) and the force to be determined (signal). The output of the block G, the deflection p is corrupted by measurement noise υ that results in the measurement y. (b) shows an experimentally obtained thermal spectra (setting $h = 0$ in the block diagram (a)) that demonstrates that the thermal response of the cantilever is discernable only near the resonant frequency of the cantilever

The resolution and the quality of the measurement method can be assessed by observing the thermal response of the cantilever. The cantilever under ambient conditions is forced by thermal noise that can be characterized as white. Equation (1) with $f(t) = \eta(t)$, a white noise input results in a power spectral density of the measured deflection y characteristic of a second order system. Figure 2 shows the power spectrum of the deflection measurement of a cantilever under ambient conditions. The only forcing on the cantilever is the white noise thermal forcing. The figure also shows a plot of second order model with the model parameters chosen to fit the measured curve near resonance. It is evident that the thermal response of the cantilever is visible near the first modal frequency (resonance) of the microcantilever whereas away from the resonance the measurement noise υ dominates the spectra. Thus the microcantilever is thermally limited near the resonance of the microcantilever. As the thermal forcing cannot be mitigated (without changing the temperature), the optimal resolution of deciphering a force on the microcantilever is given by the thermal spectra. Thus the conclusion can be reached that the optimal resolution is obtained for forces that have frequency content near the resonance of the microcantilever.

The state space representation of the cantilever dynamics is given by,

$$\begin{aligned} \dot{\overline{x}} &= A\overline{x} + B(\eta + w), \\ y &= C\overline{x} + \upsilon, \end{aligned} \tag{3}$$

where η is the thermal noise component and w describes all external forces acting on the cantilever other than the thermal noise force. For the one mode approximation, the state $\overline{x}_1$ denotes the cantilever-tip position (p), state $\overline{x}_2$ denotes the cantilever-tip velocity. The cantilever model described above can be identified precisely (see Ref. Salapaka et al. (1997)). Typical external forces on the cantilever apart from the thermal noise force are the tip-sample interaction force $h = \phi(p, \dot{p})$, the dither forcing $g(t)$ and possibly a control input $u_c(t)$.

It is to be noted that the cantilever admits a precise characterization as a finite dimensional, linear, time-invariant and causal system. This view proves crucial to the controls and systems perspectives.

2.2 Models of tip-sample interaction potential

The interaction force between the tip and the sample when viewed as an atom-atom interaction is well characterized by the Lennard-Jones force $F(r)$ given by

$$F(r) = -\frac{6A}{r^7} + \frac{12B}{r^{13}},$$

where r is the separation between the atoms (Figure 3). The term $-A/r^7$ models the Van der Waals interaction that results in an attractive force between the atoms. The effect of the repulsive forces is captured by the term $\frac{B}{r^{13}}$ in the Lennard-Jones force. Israelachvili (1985) is good reference for various surface interactions. The Lennard-Jones model provides a good qualitative characterization of the tip-sample interaction that is typically characterized by weak long-range attractive forces and strong short range repulsive forces.

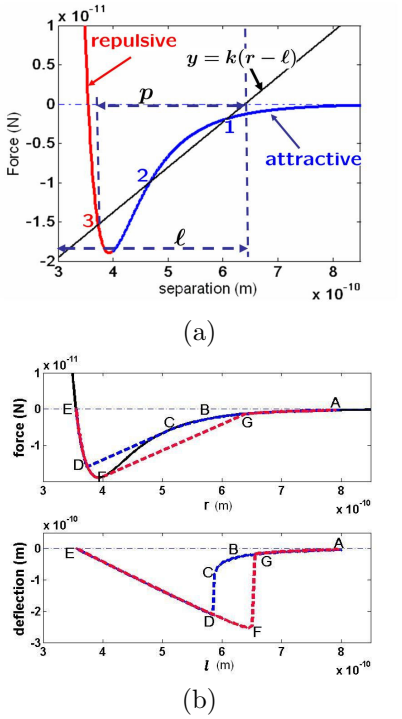

Fig. 3. (a) shows a Lennard-Jones force variation with separation (b) shows the equilibrium deflection position as the cantilever sample separation is reduced under a tip-sample potential that is governed by the Lennard Jones potential. The hysteretic behavior is observed in experiments.

The cantilever tip experiences the tip-sample interaction force characterized by the Lennard-Jones type behavior and also the restoring force due to the cantilever stiffness (k). The deflection of the cantilever when no other forces are present is governed by the balance of the spring force and the tip-sample interaction force. In Figure 3(a), for a particular offset ℓ between the cantilever base and the sample, the spring force given by $k(r-\ell)$ and the Lennard-Jones force are shown. The intersection of these curves provides the possible equilibrium states that the cantilever tip can take. In the figure three possible equilibrium positions are shown as possible. It can be shown that a particular equilibrium position is stable only if $\frac{\partial F}{\partial r} < k$ where F and k are the tip sample force and the stiffness of the cantilever. Thus equilibrium positions 1 and 3 in the figure are stable whereas 2 (in the attractive regime) is not. It is clear that if the cantilever is soft (small k) then the equilibrium positions in the attractive part will be unstable and thus the cantilever-tip cannot remain in the attractive part. Note that position 1 is too far from the sample and is almost equivalent to having no sample effects at all.

Figure 3(b) shows the various stable equilibrium deflection values that the cantilever tip assumes as the offset ℓ between the cantilever and the sample is first decreased slowly, in the approach phase, and then increased back to the original offset in the retract phase. In the approach phase, the deflection follows the curve A-B-C-D-E and the retract phase the curve is given by E-F-G-A. This type of hysteretic behavior routinely seen in experiments demonstrates complex multi-valued behavior of the system (see Wisendanger (1994)).

2.3 The force balance principle and the static mode of AFM operation

As discussed above, the tip-sample interaction potential has complex nonlinear characteristics that is also not monotonic. Apart from the multivalued behavior established in the earlier section, the nonlinear characteristic of the tip-sample interaction force leads to complex behavior (see Ashhab et al. (November 1999.), Ashhab et al. (1999), Burnham et al. (1995) and Salapaka et al. (2001)). The operation becomes more complex as the topographic image as a function of the lateral coordinates x, y is sought. The tip-sample interaction profile at different lateral positions will be different with the sample at one lateral coordinate raised or lowered with respect to another lateral position. This has the effect of a different tip-sample offset ℓ at different lateral positions. Thus the cantilever tip encounters different tip-sample interaction profiles as the sample is laterally positioned by the positioner. The force balance

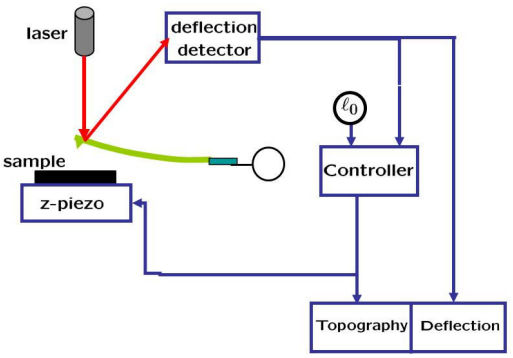

Fig. 4. Shows the static mode operation of the AFM where the deflection is regulated to maintain a set tip-sample separation ℓ_0. In this strategy the control signal provided to the vertical piezo-positioner, moves the sample in the vertical z direction to regulate the desired setpoint. The control signal is interpreted to be the topographic image.

principle also used in the Nobel prize winning invention of the STM, addresses this problem by utilizing feedback. In this principle, the piezo positioning system is actuated by the controller with the objective of regulating a desired set-point deflection (see Fig. 4). If the controller is designed well and the bandwidth/resolution demands are reasonable, then the controller maintains the cantilever-tip near a fixed operating point on the tip-sample interaction curve with small deviations from the operating condition by moving the sample with respect to the cantilever support in the vertical z direction. Thus effectively the control action prevents the cantilever tip from huge excursions and the highly nonlinear characteristics can be replaced with a linearized behavior at the operating point on the tip-sample interaction curve. In this operation, the control signal (appropriately scaled) given to the piezo (that characterizes the vertical motion of the piezo positioner) imparted by the controller to effectively counteract the topography is considered to be the topography of the sample. This ingenious method effectively negates the adverse

effects of the nonlinearities. This mode of AFM operation is termed the static mode operation of the AFM, also known as the contact mode operation of the AFM.

Notice that from earlier discussion, the following observation follows. In the static mode operation the signal detection occurs primarily in the low frequency regime and thus the measurement noise has to be overcome by the signal to be detected. Thus the forces due to the sample need to cause a deflection large enough to overcome the measurement noise in the low frequency regime where the AFM is not thermally limited. Thus the cantilever needs to have small stiffness. Thus, from the discussion on tip-sample interaction forces, it follows that the static mode operation is largely restricted to the repulsive part of the tip-sample interaction curve.

2.4 Dynamic mode atomic force microscopy

In the dynamic mode operation the cantilever is forced, typically at the first resonant frequency of the cantilever. The sample information is gleaned by monitoring the changes in the oscillations of the micro-cantilever. Typically, the information is obtained by analyzing the fundamental harmonic of the cantilever oscillation (fundamental frequency of the forcing).

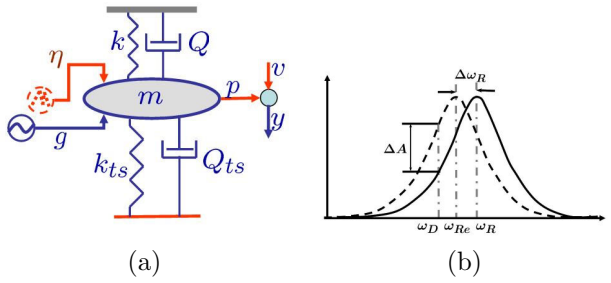

(a) (b)

Fig. 5. (a) shows that the sample effects can be viewed as a nonlinear spring forcing of the cantilever mass where k_{ts} is the nonlinear spring constant and Q_{ts} is the nonlinear quality factor (b) shows the curves of the amplitude of the first harmonic of the cantilever oscillations with respect to the frequency of the dither forcing of the cantilever. The solid and the dotted curves show the amplitude-frequency relationship when no sample is present and with sample present respectively. The frequency shift and the amplitude shift are given by $\Delta\omega_R$ and ΔA respectively when the drive frequency is ω_D.

The dynamic operating modes exploit the high SNR (signal to noise ratio) near resonance of the cantilever by shifting the information about the sample from the low frequency range (as is the case with the static mode) to a frequency range near resonance where the detection is thermally limited.

This modulation of information to a higher frequency can be understood from the following. The cantilever can be considered to be a flexure with one end being forced sinusoidally while the tip end experiences forces due to the sample. The sample can be thought as a nonlinear spring that alters the boundary condition of the flexure (see Fig. 5(a))and thereby effects the fundamental frequency of the cantilever. This viewpoint, though approximate, leads to a shift of the magnitude part of the Bode plot as shown in Fig. 5(b). Fig. 5(b) shows the Bode plot when there is no sample present with a resonant frequency ω_R. The presence of the sample alters the equivalent stiffness and the equivalent resonant frequency shifts to ω_{R_e} that leads to resonant frequency shift of $\Delta\omega_R$. If the drive frequency is ω_D then the presence of sample will lead to a change of amplitude shown by ΔA. Thus the sample effects are mapped to $\Delta\omega_R$ and ΔA both values that are present near the resonance of the cantilever. The above explanation is crude as the cantilever when oscillating traverses the entire tip-sample nonlinear regime and the simplistic concept of a nonlinear spring and damper at the tip-end of the cantilever does not illuminate the complexity of the dynamics. Averaging and other asymptotic methods (see Bogoliubov and Mitropolskii (1961)) are reported by the controls and systems community as well as the physics community (see Wang (1998), Sebastian et al. (June 1999), García and Pérez (2002) for early work in this area). There are two primary dynamic mode methods: the amplitude modulation AFM that exploits the change in amplitude (ΔA) of the first harmonic due to sample effects and the frequency modulation AFM that exploits the change in equivalent resonant frequency ($\Delta\omega_R$) due to sample effects for imaging purposes.

Amplitude modulation AFM In the AM-AFM technique, the amplitude and phase of the first harmonic of the cantilever trajectory is obtained. As is the case with the static mode, the dependence of amplitude and the phase is multi-valued with two different amplitudes (phase) possible at the same separation (see Fig. 6(b)). These multi-valued plots are not as straightforward to explain as is the case with the static modes. However, using averaging and asymptotic theory (see Bogoliubov and Mitropolskii (1961)) such plots can be understood (see Sebastian and Salapaka (2004) and Sebastian et al. (2007)).

In the most prevalent mode of AM-AFM operation the force balance principle is utilized (see Fig. 6(a)). The amplitude of the first harmonic is compared with a setpoint amplitude and the controller positions the sample vertically to maintain the setpoint. The control signal given to the vertical z positioner forms the topographical image of the sample.

In contrast to static mode imaging, in the AM-AFM imaging, the tip explores the sample only once every period. Typical amplitudes of oscillations are in the 2-50 nm range. The tip-sample interaction regime is effective over $2-10$ nm. AM-AFM method is used to image samples that have relatively large (in tens of nm) topographic variation. The AM-AFM operation is robust and is well suited for operation under fluids.

One of the significant drawbacks of the AM-AFM method is the small bandwidth. Consider the dynamics of the cantilever as given by (1). It can be shown that the solution to this dynamics when $f(t) = \gamma \sin \omega_0 t$ (with thermal noise $\eta = 0$) is of the form

$$p(t) = \overbrace{A_0 \sin(\omega_0 t + \nu_0)}^{steady\ state} + \overbrace{A' e^{-\frac{\omega_0 t}{2Q}} \sin(\omega' t + \nu')}^{transient},$$

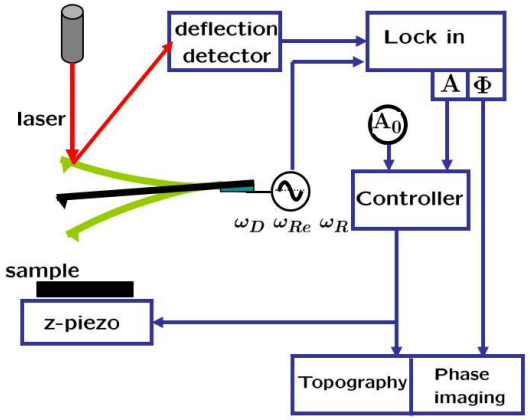

(a)

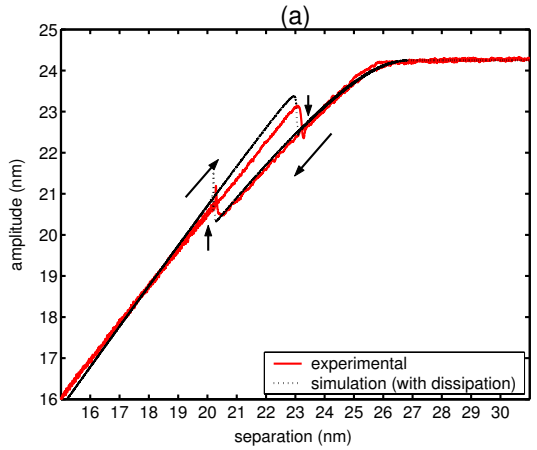

(b)

Fig. 6. (a) shows the block diagram of the amplitude modulation AFM operation. The amplitude (A) and phase (Φ) of the first harmonic are found by finding the in-phase and quadrature components by passing the deflection signal through the lock-in block. The measured amplitude is compared with a set-point amplitude A_0 that is regulated by the controller. The control signal provides the vertical motion signal to the piezo positioner that forms the topographical image. (b) shows the amplitude of the first harmonic of the cantilever deflection as the separation of the cantilever and the sample is reduced in a quasi-static manner. The sample is first brought closer to the sample in the approach phase and it is moved away from the sample in the retract phase. The approach phase and the retract phase do not overlap producing a hysteretic curve as shown.

where $\omega' = \omega_0\sqrt{1-1/4Q^2}$ with ν' and A' determined by the initial conditions of the cantilever. Evidently the transient term decays as $e^{-\frac{\omega_0 t}{2Q}}$. The time taken to reach the steady state amplitude scales linearly with the quality factor Q. This implies that for a quality factor of 500 (a representative value for operation in air) the cantilever will take approximately 500 cycles to reach the steady state. Thus methods that are based on steady state amplitude and phase are inherently slow. This is well illustrated by the simulation in Fig. 7(a) that describes the response of the cantilever system ($f_0 := \frac{\omega_0}{2\pi} = 74\ KHz$ and

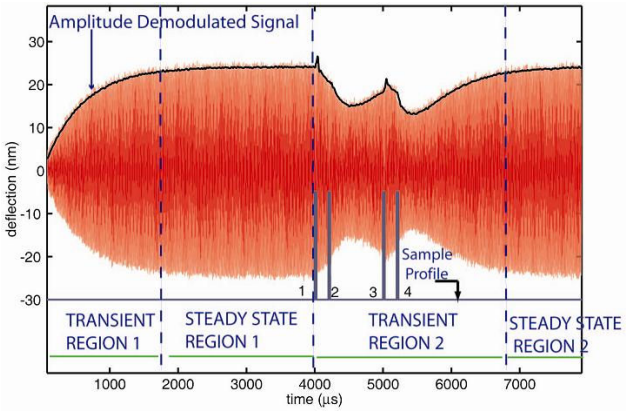

(a)

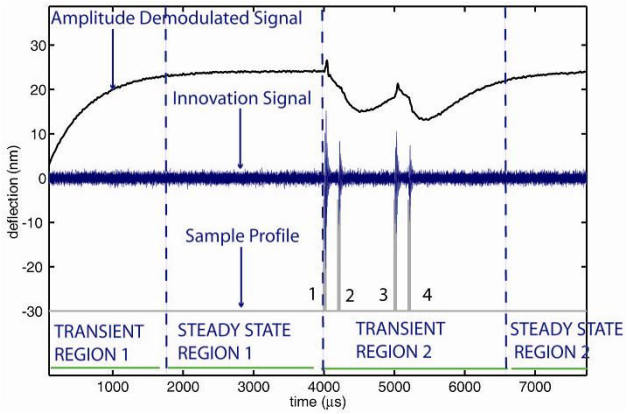

(b)

Fig. 7. (a) shows that the amplitude based signal cannot discern the hits 2, 3 and 4. (b) Shows that the innovation signal e is near zero throughout the simulation time except for four spikes when features 1, 2, 3 and 4 are introduced. As soon as the cantilever encounters feature 1, the innovation signal loses its near zero nature and takes a high value. However, after the encounter with feature 1 the near zero value is achieved fast as the observer has learned what has happened to the cantilever through the photodiode measurement in a few cycles. Similarly, features 2, 3 and 4 are detected as deviations from the near zero nature of the innovation signal. Features 1 and 2 are separated by 100 μs. This implies 10,000 features per second detection rates.

$Q = 130$) when a sinusoidal forcing at resonant frequency ω_0 is applied to the cantilever. It takes the cantilever approximately $1800\mu s$ to reach the steady state amplitude of $24nm$ from zero initial conditions. After reaching steady state it remains in this state till feature 1 in introduced. Subsequently features 2, 3 and 4 are introduced during the transient region 2. Note that the effect of feature 2, 3 and 4 are not discernable from the amplitude signal as the transient effect of the previous features clouds the effect of the subsequent features clearly demonstrating that the amplitude based method is limited in bandwidth. It is to be noted that high Q operation results in higher resolution. Indeed Angstrom resolution is possible with high Q operation Giessibl et al. (2000). Clearly amplitude based interrogation becomes impractical for such cases where the bandwidth for amplitude based detection becomes

unacceptable low. The bandwidth-resolution tradeoff that seems inherent in the above framework can be effectively addressed, for data storage applications, if the model of the cantilever is employed in real-time.

Frequency modulation AFM The Frequency Modulation AFM (FM-AFM) method provides increased sensitivity through the use of higher quality factor without compromising bandwidth. In this method, the cantilever is made to oscillate at the equivalent resonant frequency by regulating a $\pi/2$ radians phase offset between its oscillations and the sinusoidal drive input to it (Figure 8). The demodulation of the cantilever deflection signal yields the equivalent resonance frequency. In this mode, the measurement bandwidth does not degrade when Q of the cantilever is increased. The controller regulates a reference frequency shift, $\Delta\omega_0$, by comparing it with the measured frequency shift $\Delta\omega$. The z-piezo positions the sample according to the error in the desired and measured frequency shifts. This scheme is limited by thermal noise and therefore enables a high resolution imaging, however, stiffness, amplitude of oscillations of the cantilever and the quality factor need to be sufficiently large for its successful operation. This scheme is typically operated under ultra high vacuum (UHV) and low temperature conditions and works well for samples that have small variation in its topography. A detailed exposition of this method can be found in the review article Giessibl (2002).

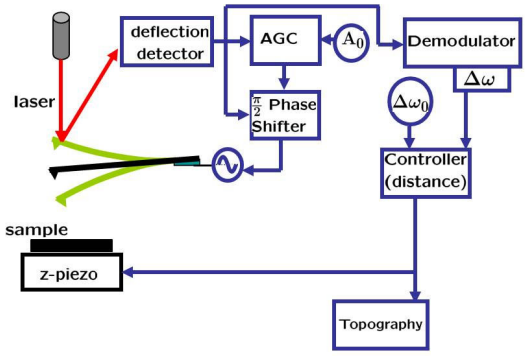

Fig. 8. FM-AFM method uses the changes in the resonant frequency of the cantilever for imaging. The cantilever when it comes under the influence of the sample behaves as an altered system with a changed equivalent resonant frequency. The cantilever is forced at its altered resonant frequency by a phase shifter circuit that maintains the forcing frequency at a phase of $\frac{\pi}{2}$ to the first harmonic phase of the deflection. The amplitude is maintained at a set value by an automatic gain controller (AGC). The sample is moved to regulate a desired shift $\Delta\omega_0$ and the control signal used forms the image of the sample.

2.5 Positioning systems

It is to be noted that the feedback mechanism in the context of SPM requires a positioning mechanism that provides resolution in the angstrom regime at an acceptable bandwidth. Piezoelectric elements provide such a high resolution positioning. Most of the current positioning systems employ a piezoelectric actuator in association with a flexure mechanism (see Figure 9 (a)). Other common types of positioning mechanisms are the cylindrical piezo configuration and the stack piezo configuration without the use of an additional flexure mechanisms.

The main challenges of piezo-actuated flexure based nanopositioners are the flexure resonances, hysteretic behavior and creep (see Fig. 9).

3. SYSTEMS APPROACHES

3.1 Nanopositioning

Lateral directions The early part of the systems and controls perspectives to AFM were primarily related to the nanopositioning aspects. The initial AFM and STM's employed feedback for the vertical direction to maintain desired set-point deflection, amplitude and frequency. However, the lateral positioning of the sample was achieved in an open-loop manner. One of the first articles that report sensing mechanisms for feedback strategies for lateral positioning is Daniele et al. (1999). One of the main contributions of this article was the sensor development for lateral sensing. The first use of modern robust control techniques for lateral positioning, primarily H_∞ control techniques can be found in Salapaka et al. (2002). Furthermore in Sebastian and Salapaka (2005), Glover-McFarlane loop shaping design (see McFarlane and Glover (1992)) was employed to shape the closed-loop maps where fundamental limitation issues were addressed. These articles established that the modern robust control tools can effectively address the issues of uncertainty, resolution and bandwidth. Furthermore they were effective in addressing the problems of nonlinear behavior of piezo actuated flexure mechanisms of hysteresis and creep.

Ultrahigh bit densities in probe-based data storage systems place significantly new challenges on nanopositioning with respect to positioning accuracy ($\approx 2nm$) over long operational periods while maintaining a fast seek time ($\leq 2ms$). Proximate-time optimal controller helps achieve fast seek times (see Sebastian et al. (2005) and Sebastian et al. (2006)) and required positioning accuracy but maintaining operations over long periods of time is still prone to ambience variations, drifts and low frequency noise effects. Media derived positional information (PES) and global positioning thermal sensor inputs have been fused to design a multiple input single output H_∞ controller to meet nanopositioning requirements by choosing best measurements in different frequency regions (see Pantazi et al. (2005) and Pantazi et al. (2007)).

Early reports of feedforward techniques to improve accuracy of positioning can be found in Croft et al. (2000). Energy based models of piezoelectric behavior that have the capability to incorporate the dependence of hysteresis loops on the frequency are developed and applied to stack and cylindrical piezos (see Hatch et al. (2006) and Smith et al. (2006)). These models based on physical principles (unlike phenomological models like the Preisach model) have the advantage of predicting more experimentally observed features that ease the implementation of inverse models for real-time purposes (see Hatch et al. (2006)). Use of charge amplifiers, another means of reducing hysteresis, can be found in Bhikkaji et al. (2007).

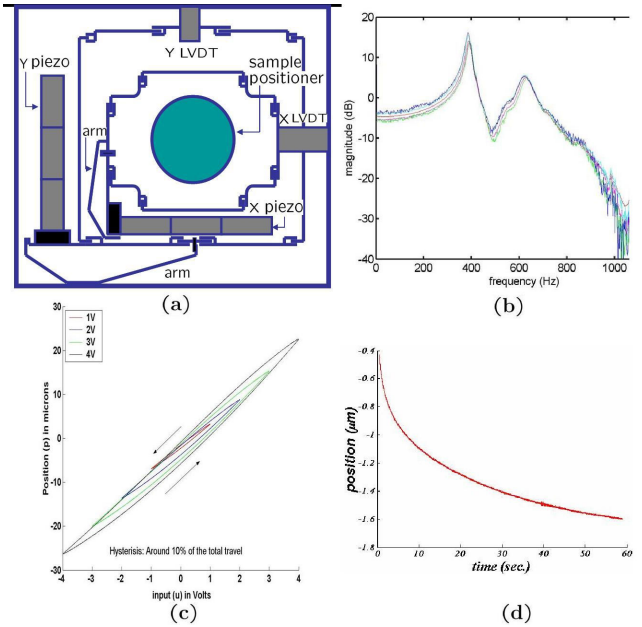

Fig. 9. (a) shows a flexure mechanism for lateral positioning of the sample (b) shows the resonances of the flexure (c) shows the hysteresis effect (d) shows the creep effects.

Nanopositioning for tip-sample separation control The force balance principle as demonstrated earlier has as an essential aspect the regulation objective of maintaining either a desired deflection, amplitude or frequency. This aspect of the AFM operation makes it possible to avoid the tip crashing into the sample and enables a "linear" analysis possible. Experimentally, the control signal in the force balance scheme provides a faithful image of the sample topography under conventional imaging conditions.

One of the earlier articles that employed modern control techniques for achieving high bandwidth regulation is Schitter et al. (2001) where a H_∞ framework was employed for controlling the vertical direction. When regulation is achieved with the sample moved at high bandwidth, then the control signal no longer provides a reliable measure of the sample topography. Thus there is a possibility of regulation objective and the image reconstruction issue being at odds. This challenge was noted in Schitter et al. (2001) and the use of observer was suggested to be pursued as future work.

The various objectives of regulation, resolution and sample reconstruction is characterized by the block diagram in Fig. 10 that illustrates that the cantilever deflection y has to be regulated at a setpoint $r = 0$. This objective is addressed by shaping the sensitivity weighting function W_S. The resolution objective is addressed by shaping the weighting on the complimentary transfer function T, given by W_T whereas the actuator saturation issues are addressed by shaping the weighting transfer function W_u. These objectives lead to the standard $S/KS/T$ control problem (see Skogestad and Postlethwaite (2005)). The important objective of sample reconstruction can be incorporated by considering the sample topography that enters the loop as a disturbance $\tilde{d}$. The sample reconstruction objective is translated to minimizing the error e_d between $\tilde{d}$ and its estimate $\hat{d}$. The result reported in Salapaka

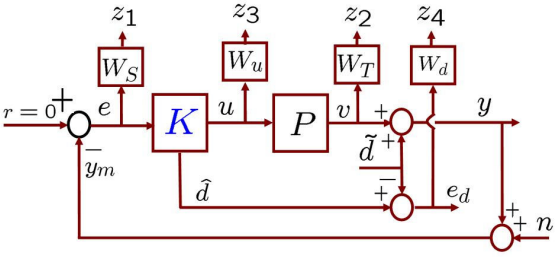

Fig. 10. Block diagram shows the various objectives important for nanopositioning and nanointerrogation. The sample profile is viewed as a disturbance $\tilde{d}$. The disturbance estimation objective is added to the standard objectives of regulation and resolution.

et al. (2005) is that the optimal H_∞ controller obtained for the stacked $S/KS/T$ stacked problem also yields the optimal estimate $\hat{d}$ of d. Thus the optimal controller with the added disturbance estimation objective is the same as the controller of the stacked H_∞ problem. Also, another important result is that the perfect estimation of the disturbance is possible. This effect of uncertainty is also studied in this article.

The effect these concepts had on the physics community is well summarized in the journal, Review of Modern Physics (see Bechhoefer (2005)).

3.2 Use of cantilever model for real-time applications

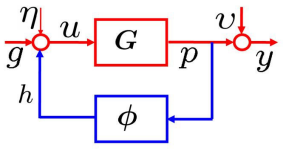

Fig. 11. Shows the feedback viewpoint to the tip-sample interaction that is viewed as an interconnection of the cantilever system G and the static nonlinear block ϕ. The interconnection is forced by a signal g and the measured signal y is the deflection. η represents the thermal noise.

The system described by (1) is viewed as an interconnection of a linear system and a nonlinear system as depicted in Fig. 11, where $h = \phi(p)$ is the sample force per unit mass. The forcing g is assumed to be sinusoidal with period T. The tip-sample interaction force appears as a feedback block. In this perspective, the instantaneous tip position is fed back to the cantilever system G through the tip-sample interaction system ϕ. The AFM dynamics are viewed as an inter-connection of two systems, the system G that models the cantilever and the block ϕ that models the sample. When the one mode model of the cantilever is assumed, the transfer function $G(s) = 1/(s^2+2\zeta\omega_0 s+\omega_0^2)$.

This systems perspective of a Lure system was introduced by the authors in Sebastian et al. (June 1999) and Sebastian et al. (June 2001) to study dynamic mode operation of AFM using harmonic and power balance tools. This viewpoint is also found in later publications in Stark et al.

(2002), Stark et al. (2004), Stark et al. (2005), and Hu et al. (2004). In Sebastian and Salapaka (August 12, 2002), the same viewpoint is employed to study the bounds on harmonics of the dynamic mode operation. In Sebastian and Salapaka (2004), the hysteretic behavior of the dynamic mode force curves using a piecewise linear model of the tip-sample interaction potential is explained.

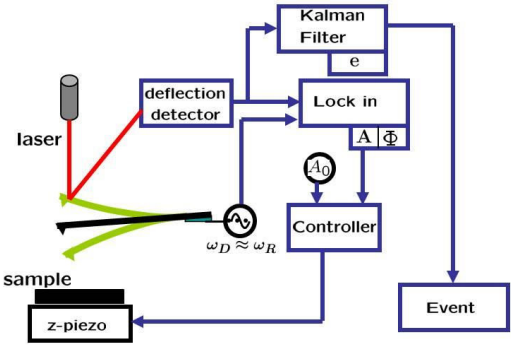

Fig. 12. The transient force atomic force microscopy (TfAfm) principle uses the model of the cantilever and employs it for an observer. The difference of the observer based estimate of the cantilever deflection and the measured deflection provides a high bandwidth means of obtaining sample information. The event block computes generalised likelihood ratio test on the innovation signal to detect the presence of hits of the tip with the sample.

As illustrated earlier, amplitude based interrogation becomes impractical for cases where the bandwidth for amplitude based detection becomes unacceptable low. The bandwidth-resolution tradeoff that seems inherent in the above framework can be effectively addressed, if the model of the cantilever is employed in real-time.

A systems viewpoint to the dynamic mode AFM is proving to be useful in devising new methods of imaging and in understanding the complex dynamics. Based on the model of the cantilever an observer to monitor the state of the cantilever can be implemented. The observer based concepts and their efficacy was reported in Sahoo et al. (2003). The observer dynamics and the associated error dynamics is given by,

$$\overbrace{\begin{array}{l}\dot{\hat{\overline{x}}} = A\hat{\overline{x}} + Bw + L(y-\hat{y}); \hat{\overline{x}}(0) = \hat{\overline{x}}_0, \\ \hat{y} = C\hat{\overline{x}},\end{array}}^{Observer}$$

$$\overbrace{\begin{array}{rl}\dot{\tilde{\overline{x}}} &= A\overline{x} + B(w+\eta) - A\hat{\overline{x}} - Bw - L(y-\hat{y}), \\ &= (A-LC)\tilde{\overline{x}} + B\eta - L\upsilon, \\ \tilde{\overline{x}}(0) &= \overline{x}(0) - \hat{\overline{x}}(0),\end{array}}^{State\ Error\ Dynamics}$$

where $\hat{\overline{x}}$ is the estimate of the state $\overline{x}$. The error in the estimate is given by $\tilde{\overline{x}} = \overline{x} - \hat{\overline{x}}$ whereas the error in the estimate of the output y is given by,

$$e = y - \hat{y} = C\tilde{\overline{x}} + \upsilon. \tag{4}$$

The error between the observed state and the actual state of the cantilever, when no noise terms or sample forces are present ($\eta = \upsilon = h = 0$) is only due to the mismatch in the initial conditions of the observer and the cantilever-tip. It is evident that if the observer gain L is chosen so that the eigenvalues of the matrix $(A - LC)$ are in the strict left half complex plane, the state error $\tilde{x}$ due to the initial condition mismatch $\tilde{x}(0)$ goes to zero with time as $e^{(A-LC)t}\tilde{x}(0)$. It can be shown that under the presence of the noise sources η and υ, the error process e approaches a zero mean wide sense stationary stochastic process after the observer has tracked the state of the cantilever. The relationship of the signal e and the initial condition reset for a one mode model is given by,

$$e(s) = \frac{\eta(s) + (s^2 + \frac{\omega_0}{Q}s + \omega_0^2)\upsilon(s) + (s + \frac{\omega_0}{Q})\nu_1 + \nu_2}{s^2 + (\frac{\omega_0}{Q} + l_1)s + (\omega_0^2 + l_2 + \frac{\omega_0}{Q}l_1)}, \tag{5}$$

where $[\nu_1,\ \nu_2]^T$ is the initial condition reset due to change in tip-sample interaction and $L = [l_1\ l_2]^T$ is the observer gain. From Equation (5) it can be seen that the tracking bandwidth B is characterized by,

$$B \propto \frac{\omega_0}{Q} + l_1. \tag{6}$$

Since the choice of the gain term l_1 in (6) is independent of the quality factor Q, the tracking bandwidth of the observer is effectively decoupled from Q. Thus the effect of the sample interaction dies out at a rate proportional to $e^{-(\omega_0/2Q+\ell_1)t}$. The limiting factor on the bandwidth of the detection of the state jump is mainly imposed by the measurement noise. Note that due to the small measurement noise, the observer gain l_1 can be chosen large enough so that the cantilever state is tracked within a couple of cycles of the dither forcing. Therefore the optimal bandwidth is primarily dictated by the resonant frequency ω_0 of the cantilever. This is in contrast to the existing steady state based detection that takes 300 cycles for a Q of 300 and 50,000 cycles for a Q of 50,000 before a new feature can be introduced and are thus fundamentally limited by Q.

One of the issues is the modelling of the force felt by the cantilever tip due to the sample. A good model of the sample interaction force h (see Fig. 11) is a train of impulses given by $\sum_i a_i\delta(t - t_i)$ where impulses occur at time t_i and the magnitude of the impulse is characterized by a_i. In this viewpoint, the sample force on the oscillating cantilever is viewed as an impulsive force that instantaneously alters the initial condition of the cantilever state. Such a viewpoint is particularly useful when the focus is on unravelling short time scale events. This viewpoint is particularly suited for high density data storage applications (see Vettiger et al. (2002) for a probe based high density data storage device). The rationale and the appropriateness of the impulse model is provided in Sahoo et al. (2005). The observer principle presented needs to be modified for imaging purposes where (See Fig. 12) the amplitude of the first harmonic is used for regulating a fixed amplitude A_0. However, the controller is used primarily to keep the cantilever engaged with the sample and to counteract the drift effects. Also, the root mean square value of the error between the observed and the measured values of the deflection is used as the imaging signal.

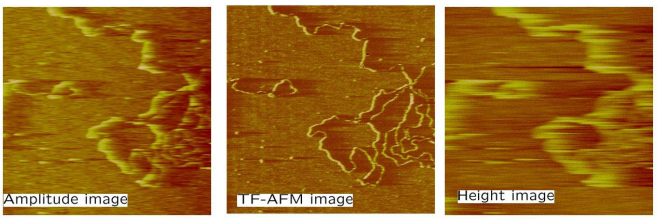

Fig. 13. Shows the images of Lambda DNA that is approx 2 nm in height. The lateral scan size is 2 μ m. The scan speed is at 12 lines per second. The figure in the middle is the transient force atomic force microscopy based image. The figures on the right and left are images obtained using traditional signals. It is evident that the TfAfm based image provides a better image in terms of having sharper contrast and reduced distortion even at high imaging speeds.

Fig. 13 shows images of DNA sample. It is evident from the images that for high bandwidth imaging TfAfm provides an attractive alternative to existing schemes.

The view of using the cantilever model also opens up new solutions to the challenging aspects of quantitative imaging where measures on the quality of the image is desired together with the image. A recent publication (see De et al. (2006)), demonstrates the efficacy of observer based perspectives for quantitative imaging. Consider the dynamics of the one mode model given by $\ddot{p} + \frac{\omega_0}{Q}\dot{p} + \omega_0^2 p = g(t) + \phi(p(t))$ where $h(t) = \phi(p(t))$ is the force on the tip due to the sample. An equivalent way of viewing the cantilever-sample interconnection described by Fig. 11 is described by the following equation

$$\ddot{p} + \frac{\omega_0'}{Q'}\dot{p} + (\omega_0')^2 p = g(t), \tag{7}$$

where

$$\omega_0'^2 = \omega_0^2 + \frac{2}{a}\frac{1}{2\pi}\int_0^{2\pi} h(a\cos\psi, -a\omega\sin\psi)\cos\psi d\psi$$

and

$$\frac{\omega_0'}{Q'} = \frac{\omega_0}{Q} + \left(\frac{1}{a\omega}\frac{1}{\pi}\int_0^{2\pi} h(a\cos\psi, -a\omega\sin\psi)\sin\psi d\psi\right).$$

Thus the cantilever-sample system can be imagined to be an equivalent cantilever system G' with forcing $g(t)$ and output $p(t)$ with modified stiffness and damping. Magnitude plots of G and G' are shown in Fig. 5(b). The equivalent stiffness and quality factor can be obtained using averaging theory and asymptotic methods (see Bogoliubov and Mitropolskii (1961)). Note that this viewpoint is different from the impulse model of the sample force. However, this viewpoint helps in quantitative imaging. As an example, consider imaging a sample with high aspect ratio. Fig. 14 (a) shows a sample with a rectangular topographic feature. The figure shows the simulated image of the rectangular profile as obtained in the AM-AFM operation (with the force balance principle) with the control signal considered as the image. It is seen that when the cantilever comes off the step and encounters a valley

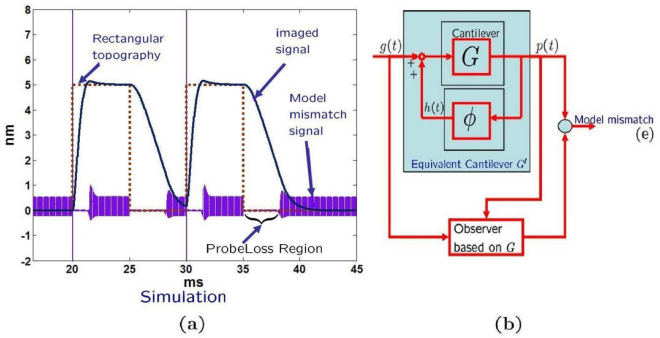

Fig. 14. (a) shows the simulation of a probe-loss situation. The sample has a rectangular profile. The image provides a wrong estimate of the sample in the probe-loss area (b) shows the architecture to detect the probe-loss situation. An observer based on the nominal model is implemented and the deflection predicted by the observer compared to the measured deflection. The difference between these signals provides the means to detect probe-loss

in the sample topography the cantilever stops interacting with the sample thus there is a loss of the probe, the cantilever. It is not possible with conventional means to detect the probe-loss condition and the image (the straight line with a slope) obtained be misinterpreted in the probe-loss situation. Probe loss situation can be detected in real-time (see De et al. (2006)). The main concept is presented in Fig. 14)(b) that shows an observer based on the nominal model G and the cantilever-sample system. The deflection as predicted by the nominal model is compared with the measured deflection. The equivalent resonant frequency of the cantilever when interacting with the sample (the model is described by G') is different from the resonant frequency of nominal model G. This mismatch in the two systems G' and G will lead to a mismatch e. When the cantilever, the probe is not interacting with the sample, the mismatch is small and thus a model-mismatch signal can be obtained. Fig. 14(a) shows such a signal and it is evident that this signal indicates the probe-loss area. Experimental corroboration of the simulation results can be found in De et al. (2006).

As the detection can be done in real-time, the probe-loss signal can be used by the controller to reduce the probe-loss effected area while being gentle to the sample. In a preliminary experiment, a switching controller was used. Fig. 15 shows the control signal as the sample, with a rectangular topographic profile, is imaged. It shows the plots with low controller gains that have large probe-loss effected area and the controller with high gains has small probe-loss effected area but it shows large overshoot that cause damage to the sample. It also shows a switched gain controller that alternates between a low gain when the probe is engaged and uses a high gain when the probe has lost the sample. This controller has the advantage of small probe-loss effected area and at the same time is gentle on the sample.

High resolution imaging A issue for high resolution imaging, particularly for applications where bandwidth needs are not stringent is that of drift. Drift processes,

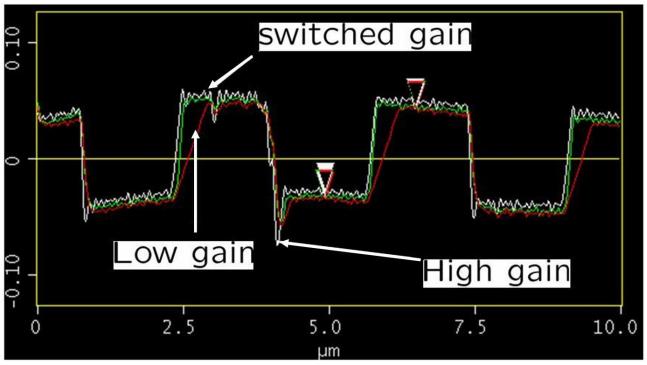

Fig. 15. The figure shows three plots for controller with low gain, high gain and switched gain. The low gain controller has high probe-loss effected area but is gentle on the sample whereas the high gain controller has low probe-loss effected area but is harsh on the sample. The switched gain controller has the advantage of being gentle on the sample and having smaller probe-loss effected area.

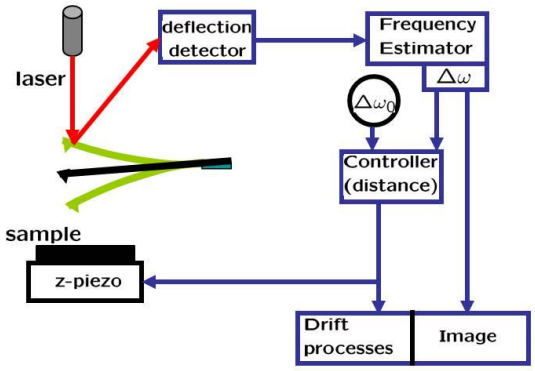

Fig. 16. Figure shows the architecture of the thermally driven non contact AFM operation where the cantilever is not forced externally using the dither piezo. The only force driving the cantilever is the thermal forcing. This white noise drive provides small motion of the cantilever. The frequency estimator evaluates the equivalent resonant frequency of the microcantilever. The equivalent resonant frequency reduces (increases) when the cantilever tip encounters the attractive (repulsive) part of the tip-sample interaction. This controller moves the sample in the vertical direction to maintain a equivalent frequency shift that is negative thereby maintaining the cantilever in the attractive part of the tip-sample interaction.

the source of which, is hard to discern make it difficult to interrogate samples for extended periods of time as the drift processes separate the probe from the sample or crash the probe into the sample.

Dynamic mode AFM where the cantilever oscillations have small amplitude have a number of advantages over large amplitude schemes (see Giessibl (2003)). An intuitive explanation is that when the cantilever oscillations are small, the cantilever remains in the tip-sample interaction potential for a larger portion of its trajectory that leads to greater shifts in the equivalent resonant frequency. The difficulty of small amplitude operation is that of stability (see Giessibl (2003)).

In thermally driven non-contact AFM (ThNcAfm), (see Gannepalli et al. (2005)) the cantilever is not forced externally using a dither. It utilizes the natural forcing provided by the thermal bath (see Fig. 16). Such a forcing induces the smallest possible oscillations of the cantilever and thus has the advantages of small amplitude AFM methods. The ThNcAfm method is fundamentally a frequency modulation AFM method which relies on the resonant frequency shift caused by the sample (see (7)). In ThNcAfm, the cantilever is forced by thermal noise. A frequency estimator is implemented that finds the peak of the power spectral density (psd) plot of the cantilever deflection measurement. Such a frequency estimator can be implemented using, for example, Pisarenko harmonic decomposition method (see Pisarenko (1973)). The peak of the psd shifts depending on the sample force (see Fig. 5). In particular, the shift is negative (positive) when the net force experienced by the cantilever is attractive (repulsive). The controller, that actuates the piezo positioner, is designed to maintain a negative frequency shift. Thus the controller acts to maintain the cantilever in the attractive part of the tip sample separation. The controller using the presented strategy effectively counteracts drift process. Drift processes are slow and therefore the bandwidth demands are not stringent. The sample information that has frequency content higher than the drift processes will not be cancelled by the controller and thus the frequency shift in the appropriate frequency range will provide the information on the sample. The above operation is also explained in Fig. 17.

The above method as is shown in Gannepalli et al. (2005), has the ability to yield sub-Angstrom resolution.

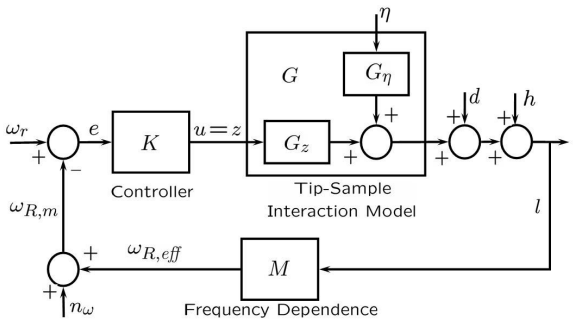

Fig. 17. A block diagram representation of the thermally driven non-contact AFM architecture is shown. η and d are the thermal noise and drift disturbances respectively. h is the sample topographical signal that needs to be imaged. G_z and G_η are the scanner and the cantilever transfer function respectively that effect the tip-sample offset ℓ. n_ω is the noise that is present in estimating the equivalent resonant frequency and ω_r is the resonant frequency to be regulated that is set below the natural resonant frequency of the cantilever.

4. FUTURE DIRECTIONS

Nanopositioning in the recent years has attracted considerable focus from the controls community. Some interesting directions that have to be investigated are the applications of MIMO designs. Considerable effort is spent in the design of nanopositioning stages to avoid the coupling of motion between various directions. MIMO design can be used to effectively design control strategies to decouple the motion in various directions thereby reducing the effort spent on the design of nanomanufacturing stages. Conceivably the relaxation on the stage design can lead to faster stages. A recent result in these directions is provided in Dong et al. (2007).

In the dynamic mode operation, it is known that the more intricate features of the tip sample force profile cannot be discerned using the first harmonic alone. This has motivated several groups to investigate and utilize the higher harmonics (see for example Crittenden et al. (2005) and Giessibl (2006)). In Proksch (2006) forcing frequencies with more than one harmonic to further enhance the higher harmonics is indicated. The study of higher harmonics and their use for imaging is a direction that remains significant. Systems approaches in estimating the magnitudes of the higher harmonics is provided in Sebastian et al. (2007).

One of the drawbacks of the AFM scheme is that it is slow when compared to for example optical imaging. It explores the sample at the small scale in a serial manner and often the objective is to image a sample with large dimensions. A strategy to overcome this drawback is that of parallelism. The probe based data storage device that IBM, Zurich research labs has pioneered (see Vettiger et al. (2002)) is an example of parallelism. The control strategies for such structures has to incorporate the information structure that the devices enforce and a means of controlling such massive systems will have to be designed and implemented. A recent result in this direction is reported by Mariateresa Napoli and Bamieh (2005).

REFERENCES

National nanotechnology initiative: The initiative and its implementation plan,. *National Science and Technology Council, Committee on Technology, Subcommittee on Nanoscale Science, Engineering and Technology, July 2000. Available at http://www.nano.gov/nni2.pdf.*

M. Ashhab, M. V. Salapaka, M. Dahleh, and I. Mezic. Dynamical analysis and control of micro-cantilevers. *Automatica*, 1999.

M. Ashhab, M. V. Salapaka, M. Dahleh, and I. Mezic. Melnikov-based dynamical analysis of microcantilevers in scanning probe microscopy. *Nonlinear Dynamics*, November 1999.

John Bechhoefer. Feedback for physicists: A tutorial essay on control. *Reviews of Modern Physics*, 77(3): 783, 2005. doi: 10.1103/RevModPhys.77.783. URL `http://link.aps.org/abstract/RMP/v77/p783`.

B. Bhikkaji, M. Ratnam, A. J. Fleming, and S. O. R. Moheimani. High-performance control of piezoelectric tube scanners. *IEEE Transactions on Control Systems Technology*, 5(5):853–866, September 2007.

G. Binnig, H. Rohrer, Ch. Gerber, and E. Weibel. Tunnelling through a controllable vacuum gap. *Applied Physics Letters*, 40(2):178–180, 1982.

N. N. Bogoliubov and Y. A. Mitropolskii. *Asymptotic methods in the theory of non-linear oscillations*. Hindustan publishing corporation, New Delhi, India, 1961.

N. A. Burnham, A. J. Kulik, G. Gremaud, and G. A. D. Briggs. Nanosubharmonics: the dynamics of small nonlinear contacts. *Physics Review Letters*, 74:5092–5059, 1995.

S. Crittenden, A. Raman, and R. Reifenberger. Probing attractive forces at the nanoscale using higher-harmonic dynamic force microscopy. *Physical Review B (Condensed Matter and Materials Physics)*, 72(23): 235422, 2005. doi: 10.1103/PhysRevB.72.235422. URL `http://link.aps.org/abstract/PRB/v72/e235422`.

D. Croft, G. Shedd, and S. Devasia. Creep, Hysteresis and Vibration compensation for Piezoactuators: Atomic Force Microscopy Application. In *Proceedings of the American Control Conference, Chicago, Illinois*, pages 2123–2128, June 2000.

A. Daniele, S. Salapaka, M. V. Salapaka, and M. Dahleh. Piezoelectric scanners for atomic force microscopes: design of lateral sensors, identification and control. In California San Diego, editor, *Proceedings of the American Control Conference*. pp. 253-257, June 1999.

Tathagata De, Pranav Agarwal, Deepak R. Sahoo, and Murti V. Salapaka. Real-time detection of probe loss in atomic force microscopy. *Applied Physics Letters*, 89(13):133119, 2006. doi: 10.1063/1.2357876. URL `http://link.aip.org/link/?APL/89/133119/1`.

Jingyan Dong, Srinivasa M. Salapaka, and Placid M. Ferreira. Robust mimo control of a parallel kinematics nano-positioner for high resolution high bandwidth tracking and repetitive tasks. *Proceedings of Control and Decision Conference*, accepted, 2007.

A. Gannepalli, A. Sebastian, J. Cleveland, and M.V. Salapaka. Thermally driven non-contact atomic force microscopy. *Applied Physics Letters*, 87(11):111901, 2005. URL `http://link.aip.org/link/?APL/87/111901/1`.

R. García and R. Pérez. Dynamic atomic force microscopy methods. *Surf. Sci. Rep.*, 47:197, 2002.

F. J. Giessibl. *Noncontact Atomic Force Microscopy*, chapter Principle of NC-AFM, page 11. NanoScience and Technology. Springer, Berlin, 2002.

F. J. Giessibl. Advances in atomic force microscopy. *Rev. Mod. Phys.*, 75(3):949, July 2003.

F. J. Giessibl. Higher-harmonic atomic force microscopy. *Surf. Interf. Anal.*, 38:16961701, 2006.

F. J. Giessibl, S. Hembacher, H. Bielefeldt, and J. Mannhart. Subatomic features on the silicon (111)-(7×7) surface observed by atomic force microscopy. *Science*, 289:422–425, July 2000.

A.G. Hatch, R.C. Smith, T. De, and M.V. Salapaka. Construction and experimental implementation of a model-based inverse filter to attenuate hysteresis in ferroelectric transducers. *IEEE Transactions on Control Systems Technology*, 14(6):1058 – 1069, 2006.

S. Hu, S. Howell, A. Raman, R. Reifenberger, and M. Franchek. Frequency domain identification of tip-sample van der waals interactions in resonant atomic force microcantilevers. *Journal of Vibration and Acoustics*, 126(3):343351, 2004.

J. N. Israelachvili. *Intermolecular and Surface Forces*. Academic Press, 1985.

Kimberly Turner Mariateresa Napoli, Wenhua Zhang and Bassam Bamieh. Characterization of electrostatically coupled microcantilevers. *Journal of Micromechanical Systems*, 14(2), 2005.

D. McFarlane and K. Glover. A loop shaping design procedure using H_∞ synthesis. *IEEE Transactions on Automatic Control*, (6):759–769, 1992.

A. Pantazi, A. Sebastian, H. Pozidis, and E. Eleftheriou. Two-sensor-based h_∞ control for nanopositioning in probe storage. *Proceedings of the IEEE Conference on Decision and Control, Seville, Spain*, pages 1174–1179, December 2005.

A. Pantazi, A. Sebastian, G. Cherubini, M. Lantz, H. Pozidis, H. Rothuizen, and E. Eleftheriou. Control of MEMS-based scanning-probe data-storage devices. *IEEE Transactions on Control System Technology*, 15(5):824–841, September 2007.

V. F. Pisarenko. The retrieval of harmonics from a covariance function. *Geophysics, Journal of Royal Astronomical Society*, 33:347, 1973.

R. Proksch. Multifrequency, repulsive-mode amplitude-modulated atomic force microscopy. *Applied Physics Letters*, 38:16961701, 2006.

D. R. Sahoo, A. Sebastian, , and M. V. Salapaka. Transient-signal-based sample-detection in atomic force microscopy. *Applied Physics Letters*, 83(26):5521, December 2003.

D. R. Sahoo, A. Sebastian, , and M. V. Salapaka. Harnessing the transient signals in atomic force microscopy. *International Journal of Robust and Nonlinear Control*, 15:805–820, 2005.

M. V. Salapaka, H. S. Bergh, J. Lai, A. Majumdar, and E. McFarland. Multi-mode noise analysis of cantilevers for scanning probe microscopy. *Journal of Applied Physics*, 81(6):2480–2487, March 1997.

S. Salapaka, M. Dahleh, and I. Mezic. On the Dynamics of a Harmonic Oscillator Undergoing Impacts with a Vibrating Platform. *Nonlinear Dynamics*, 24:333–358, 2001.

S. Salapaka, A. Sebastian, J. P. Cleveland, and M. V. Salapaka. High bandwidth nano-positioner: A robust control approach. *Review of Scientific Instruments*, 73: 3232–3241, 2002.

S. Salapaka, T. De, and A. Sebastian. Sample-profile estimate for fast atomic force microscopy. *Applied Physics Letters*, 87:053112, 2005.

D. Sarid. *Scanning Force Microscopy with applications to Electric, Magnetic and Atomic Forces*. Oxford University Press, 1991.

G. Schitter, P. Menold, H. F. Knapp, F. Allgower, and A. Stemmer. High performance feedback for fast scanning atomic force microscopes. *Review of Scientific Instruments*, 72(8):3320–3327, August 2001.

A. Sebastian and M.V. Salapaka. Analysis of Periodic Solutions in Tapping Mode AFM. *Mathematical Theory of Networks and Systems, University of Notredame, South Bend, Indiana*, August 12, 2002.

A. Sebastian and M.V. Salapaka. Amplitude Phase Dynamics and Fixed Points in Tapping-Mode Atomic Force Microscopy. *Proceedings of the American Control Conference, Boston, Massachusetts*, pages 2499–2504, June 30 - July 2 2004.

A. Sebastian and S. Salapaka. Design methodologies for robust nano-positioning. *IEEE Transactions on Control Systems Technology*, 13(6):868–876, 2005.

A. Sebastian, A. Pantazi, G. Cherubini, E. Eleftheriou, M. A. Lantz, and H. Pozidis. Nanopositioning for probe storage. *Proceedings of the American Control Conference,Portland, Oregon*, pages 4181–4186, 8-10 June 2005.

A. Sebastian, A. Pantazi, G. Cherubini, M. Lantz, H. Rothuizen, H. Pozidis, and E. Eleftheriou. Towards faster data access: Seek operations in mems-based storage devices. *Proceedings of the IEEE Conference on Control Applications, Munich, Germany*, pages 283–288, October 2006.

A. Sebastian, A. Gannepalli, and M. V. Salapaka. A review of the systems approach to the analysis of dynamic-mode atomic force microscopy. *IEEE Transactions on Control System Technology*, 15(5):952–959, 2007.

A. Sebastian, M. V. Salapaka, D. Chen, and J. P. Cleveland. Harmonic balance based analysis for tapping-mode AFM. *Proceedings of the American Control Conference, San Diego*, pages 232–236, June 1999.

A. Sebastian, M. V. Salapaka, D. Chen, and J. P. Cleveland. Harmonic and power balance tools for tapping-mode atomic force microscope. *Journal of Applied Physics*, 89 (11):6473–6480, June 2001.

S. Skogestad and I. Postlethwaite. *Multivariable Feedback Control*. John Wiley and Sons, 2005.

Ralph C. Smith, Andrew G. Hatch, Tathagata De, Murti V. Salapaka, Ricardo C. H. del Rosario, and Julie K. Raye. Model development for atomic force microscope stage mechanisms. *SIAM Journal on Applied Mathematics*, 66(6):1998–2026, 2006. doi: 10.1137/05063307X. URL `http://link.aip.org/link/?SMM/66/1998/1`.

M. Stark, R. Guckenberger, A. Stemmer, and R. W. Stark. Estimating the transfer function of the cantilever in atomic force microscopy: A system identification approach. *Jounal of Applied Physics*, 98:114904 1–7, 2005.

R. W. Stark, G. Schitter, M. Stark, R. Guckenberger, and A. Stemmer. State-space model of freely vibrating and surface-coupled cantilever dynamics in atomic force microscopy. *Physical Review B*, 69(8):085412.1–9, 2004.

R. W. Stark, M.and Stark, W. M. Heckl, and R. Guckenberger. Inverting dynamic force microscopy: From signals to time-resolved interaction forces. *Proceedings of the National Academy of Science*, 99(13):8473–8478, 2002.

P. Vettiger, G. Cross, M. Despont, U. Drechsler, U. Durig, B. Gotsmann, W. Haberele, M. A. Lantz, H. Rothuizen, R. Stutz, and G. Binnig. The millipede-nanotechnology entering data storage. *IEEE Transactions on Nanotechnology*, 1((1)), 2002.

L. Wang. Analytical descriptions of the tapping-mode atomic force microscopy response. *Applied Physics Letters*, Volume 73, Number 25:3781–3783, 1998.

R. Wisendanger. *Scanning Probe Microscopy and Spectroscopy*. Cambridge University Press, 1994.